36.0 RATIONALIZATION OF LIQUID/SOLID AND SOLID/SOLID INTERFACE INSTABILITIES DURING THERMAL – MECHANICAL TRANSIENTS OF METAL ADDITIVE MANUFACTURING

Alec Saville (Mines)
Faculty: Amy Clarke (Mines)
Other Participants: Jonah Klemm-Toole (Mines)
Industrial Mentor: TBD

This project initiated in Fall 2018 and is supported by the Office of Naval Research. The research performed during this project will serve as the basis for an M.S./Ph.D. thesis for Alec Saville.

36.1 Project Overview and Industrial Relevance

Additive manufacturing (AM) of metallic alloy systems has been a topic of growing interest in the materials and manufacturing communities. Due to the large thermal gradients (10^3-10^7 $\frac{K}{m}$) and rapid rate at which these gradients can reverse signs during AM (> 10 Hz), steady state assumptions about solidification behavior used in traditional processes may not apply as seen in **Figure 36.1**. The liquid/solid and solid/solid interfacial instabilities that can emerge are not well understood, and may result in deleterious microstructural and defect evolution, including porosity and unwanted anisotropy for example [36.1]. Therefore, the prediction and control of such phenomenon is key to ensuring proper material performance in AM, and can assist in developing qualification and certification methodologies for meeting performance criteria during printing of AM components [36.2].

This project focuses on using samples of Ti-6Al-4V and Inconel 738 manufactured with electron beam melting (EBM) to probe the aforementioned issues. Varying scan strategies were implemented in the production of these samples in order to analyze how instabilities evolve with different AM parameters and local thermal histories. The effects that instabilities have on texture evolution, microstructure, phase fractions, defect formation, and resultant material performance will all be investigated via *in-situ* and *ex-situ* characterization, as detailed later in this report. The culmination of these investigations will elucidate how spatial and temporal transients and interfacial instabilities impact microstructural and defect evolution during AM.

36.2 Previous Work

This project started in Fall 2018 and involves collaboration with the University of Tennessee, Iowa State University, The Ohio State University, Virginia Tech, the University of California Santa Barbara, the University of Sydney, and the University of New South Wales via a Multidisciplinary University Research Initiative (MURI) supported by the Office of Naval Research (ONR). Ti-6Al-4V samples (15 mm x 15 mm x 25 mm^3) were produced with DeHoff, Linear Raster, and Random scan modes via EBM at the University of Tennessee (UT), and are shown in **Figure 36.2.**

The most complex strategy, the DeHoff method involves only melting material every 11 voxels per row. This process is then repeated by shifting the melt location over one voxel and repeating for each row until the entire layer has been completed. Linear Raster melts material in a complete linear path from one side of the sample to the other during the build process, while Random melts material in each layer's voxels randomly until layer completion. It is worth noting that both the DeHoff and Random scan strategies melt in local spots, while Linear Raster material melts each layer in lines. Thus, each scan strategy varied the local thermal history and changed the evolution of instabilities throughout each build. An Inconel 738 sample was also produced using the Random scan strategy. Linear raster and DeHoff builds of Inconel 738 will be received at a later date.

Each Ti-6Al-4V specimen was sectioned lengthwise. One half remained at the Colorado School of Mines (Mines) for study, while the other half was sent to Los Alamos National Laboratory (LANL) for High-Pressure-Preferred-Orientation (HIPPO) neutron beamline measurements. **Figure 36.3** shows a schematic drawing of the detectors in the HIPPO instrument. Neutron diffraction using the HIPPO beamline allows for a much greater penetration depth than with x-rays, due to the use of a high energy neutron source [36.3]. Data was collected at HIPPO using 1200 ^{3}He detectors to capture neutron scattering events and determine crystallographic orientation. The data was output as a series of separate datafiles for Rietveld refinement. "Bulk" texture measurements were made at the center of each

build, whereas "local" texture measurements were made along the build length in 2 and 4 mm increments for each scan strategy. The data was refined using the software Material Analysis Using Diffraction (MAUD).

36.3 Recent Progress

36.3.1 Literature Review

Literature review of phase transformations and microstructural evolution in Ti-6Al-4V and Inconel 738 and regarding AM processes in general is underway, in conjunction with analyzing texture data. Recent effort has focused on insights into variant selection in Ti-6Al-4V, the effects of AM build strategy on the $\beta \rightarrow \alpha$ phase transformation, and the influence of AM on texture evolution along the length of the build.

36.3.2 Analyzing Bulk Texture Profiles

After processing the bulk texture data, analysis of the results indicated a clear variation in α and β textures between each scan strategy. Pole figures corresponding to the α and β phases for each scan strategy are shown in **Figure 36.4**. The Random strategy exhibited a relatively strong (0002) α phase texture, roughly 45 degrees from the build direction, with an observed maximum intensity of approximately 4 multiples of a random distribution (mrd). The DeHoff scan strategy showed a similar (0002) α phase texture, with a maximum intensity of approximately 3 mrd. The Raster strategy also showed a similar (0002) α phase texture, but the intensity was the lowest with a maximum value of approximately 2 mrd. The Raster strategy showed (0002) α phase intensities closer to a random distribution of crystallographic orientation for angles far away from the build direction, whereas the other two scan strategies showed intensities lower than a random distribution for large angles from the build direction. The β pole figures were all normalized to 7 mrd to illustrate differences in areas of preferred orientations, and to observe potential evidence of $\beta \rightarrow \alpha$ transformation (via the ring-like intensities) arising from the Burger's orientation relationship, where the β phase {110} family of planes are parallel to the (0002) plane of the α phase [36.4].

Initial investigations suggest the Linear Raster scan strategy reduces the propensity of preferred orientations and/or limits transformation events seen in the other scan strategies. This series of experiments only collected the average bulk texture by analyzing an area roughly in the middle of each build section. Additional neutron diffraction measurements were made to measure texture as a function of build height.

36.3.3 Local Texture Profile Experiments

Each Ti-6Al-4V sample was subjected to a series of local-texture experiments with the HIPPO neutron beamline at LANL. Instead of analyzing the "bulk" texture of each specimen, the neutron beam was allowed to only interact with a specified region of material via the use of a slit-beam guard. A small slit opening allows for a restricted flux of incident neutrons, while the guard material blocks the remaining beam. The slit-guard assembly is held statically in the sample chamber, while each specimen is held upside down and is raised/lowered by 2-4 mm intervals to analyze a target area.

Pole figures corresponding to three planes of the α phase for each scan strategy are shown in **Figures 36.5, 36.6,** and **36.7,** which correspond to 1, 13, and 24 mm heights in each sample, respectively. It is worth noting that no β texture profiles are included here, as the results exhibit statistical uncertainty due to the small amounts present in the microstructure. The β texture likely warrants further investigation via other methods like electron backscatter diffraction.

At 1 mm above the initial build surface, the Linear Raster strategy exhibited the highest intensity of (0002) texture of all three methods, with a highly clustered distribution of preferred orientations, as shown in **Figure 36.5**. This is likely evidence of columnar and oriented growth during solidification of the β phase, stemming from the initial deposition process [36.5]. Evidence of a similar (0002) texture is seen with the Dehoff scan strategy, indicating some similarity in the solidification conditions within this region of deposition. The Random scan strategy produced a (0002) texture with a lower maximum intensity compared to the other strategies. The (0002) texture observed with the Random scan strategy at a height of 1 mm more closely resembles the corresponding bulk value. However, considerable differences are observed between the bulk texture and texture measured at 1 mm above the initial build surface for the Dehoff and

Linear Raster strategies.

At 13 mm above the start of the build, the texture of each scan strategy evolves considerably (**Figure 36.6**). The textures exhibited midway along the build by the Linear Raster and DeHoff scan strategies differ from those near the start of the build. The Random scan strategy exhibited an α texture similar to that seen in the bulk texture measurement, unlike the other two strategies. Both DeHoff and Linear Raster exhibited a much lower α intensity than at 1 mm, indicating a change in preferred orientation during solidification or the during $\beta \rightarrow \alpha$ transformation. This phenomenon is not be observed in the Random spot scan strategy likely due to differences in the thermal gradients found during the build process, and is the topic of future work.

At 24 mm from the start of the build, the Dehoff and Linear Raster scan strategies again display differences in texture compared to other locations in the build, as shown in **Figure 36.7**. The textures exhibit some similarity to those observed midway along the build height, but now exhibit higher local intensities. The Random scan strategy exhibits a similar α texture profile as seen in the 13 mm height and bulk experiments, indicating consistent thermal gradients during this portion of the solidification process and during the $\beta \rightarrow \alpha$ transformation. The consistency of texture is of potential importance in a large number of applications, where the ability to effectively create parts with controlled orientations is desired. The variability of the DeHoff and Linear Raster scan strategies also opens up avenues to potentially alter the microstructure locally, but requires further investigation to evaluate. Correlations to local thermal conditions and complementary electron microscopy is underway.

36.3.4 Experiments at the Advanced Photon Source

Beam-time was recently allocated to this project to analyze solidification in real-time during simulated AM conditions with synchrotron x-ray imaging and diffraction at Sector 32-ID-B at the Advanced Photon Source (APS) at Argonne National Laboratory (ANL). Experiments included studying the solidification of Ni-Al-Mo ternary alloy single crystals with varying orientations, and observing the influence of build conditions on solidification during spot and raster experiments. Inconel 718 and 738 were also imaged during simulated AM. Results from this work will be discussed in the next reporting period.

36.4 Plans for Next Reporting Period

The bulk and local neutron texture measurements have illustrated a clear difference in the texture evolution along the build height associated with each scan strategy. The tasks planned for the next reporting period include:

- Processing of the APS experimental data on nickel alloy single crystal samples and complementary post-mortem electron microscopy.
- Determination of β texture from α orientation distribution functions acquired from MAUD in Ti-6Al-4V.
- Linking texture evolution in the Ti-6Al-4V samples to the local build conditions for the three different scan strategies used.
- Perform neutron diffraction measurements on Inconel 738 specimens built with different scan strategies.
- Complementary microstructural characterization of the Ti-6Al-4V specimens to link local microstructural to the local texture results.
- Attend and present at the Additive Manufacturing and Powder Metallurgy (AMPM) 2019 Conference.
- Prepare a peer-reviewed journal article on the Ti-6Al-4V texture results.

36.5 References

[36.1] S.J. Foster, K. Carverr, R.B. Dinwiddie, F. List, K. A. Unocic, A. Chaudhary, S.S. Babu, Process-Defect-Structure-Property Correlations During Laser Powder Bed Fusion of alloy 718: Role of In Situ and Ex Situ Characterizations, Metallurgical and Materials Transactions A. Online (2018).

[36.2] S.S. Babu, A. Clarke, et. al, MURI AM Project Narrative v.1.1, University of Tennessee, 2017.

[36.3] S.C. Vogel, S. Takajo, M.A. Kumar, E.N. Caspi, A. Pesach, E. Tiferet, O. Yeheskel, Ambient and High-Temperature Bulk Characterization of Additively Manufactured Ti-6Al-4V Using Neutron Diffraction, The Journal of the Minerals, Metals, and Materials Society. Online (2018).

[36.4] N. Gey and M. Humbert, Characterization of the variant selection occurring during the α→β→α phase transformations of a cold rolled titanium sheet, Acta Materialia. 50 (2002) 277–287. doi:10.1016/S1359-6454(01)00351-2.

[36.5] A.A. Antonysamy, J. Meyer, P.B. Prangnell, Effect of build geometry on the β-grain structure and texture in additive manufacture of Ti6Al4V by selective electron beam melting, Materials Characterization. 84 (2013) 153–168. doi:10.1016/j.matchar.2013.07.012

36.6 Figures and Tables

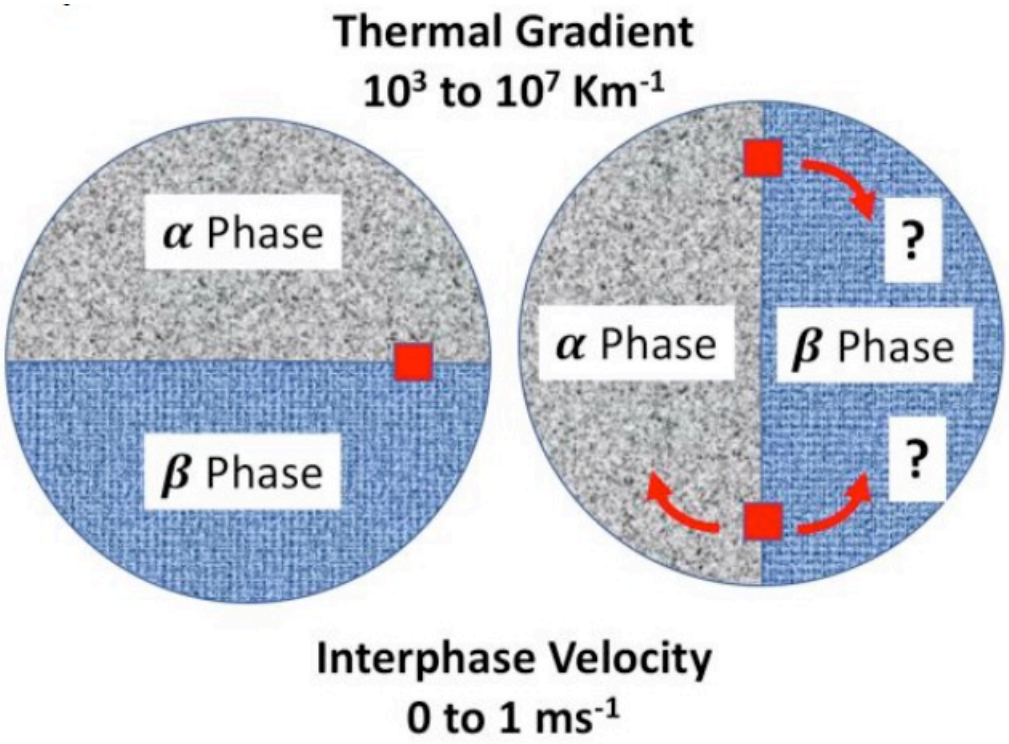

Figure 36.1: Illustration depicting an example of dynamic interphase boundaries present during AM processing.

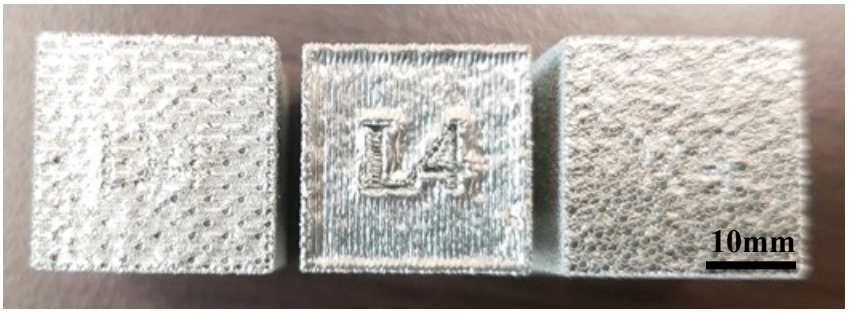

Figure 36.2: Photo of Ti-6Al-4V samples before sectioning. Note the different scan strategies as exhibited by the surface topography of the DeHoff scan strategy (left), the Linear Raster scan strategy (center), and Random (right).

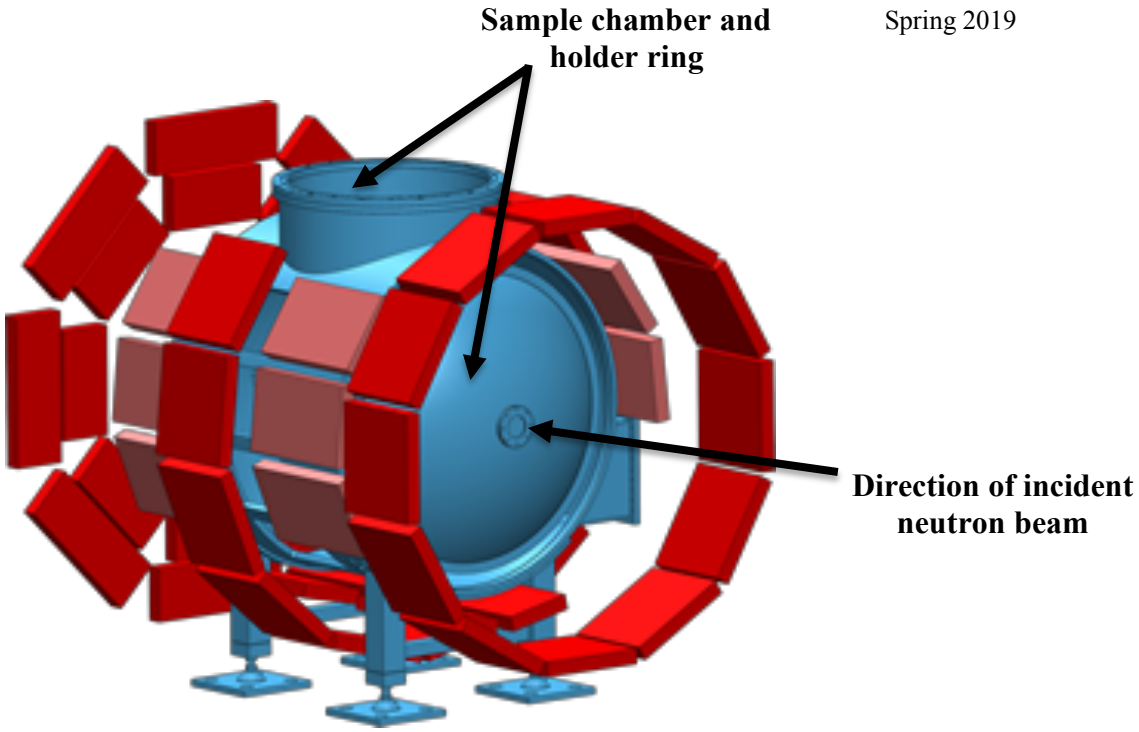

Figure 36.3: Rendering of the HIPPO beam line ^{3}He sensor arrays and sample chamber used in collection of texture data in this project. Samples are held upside-down in the center of the sample chamber via a robotic arm connected to the ring structure depicted at the top of the illustration.

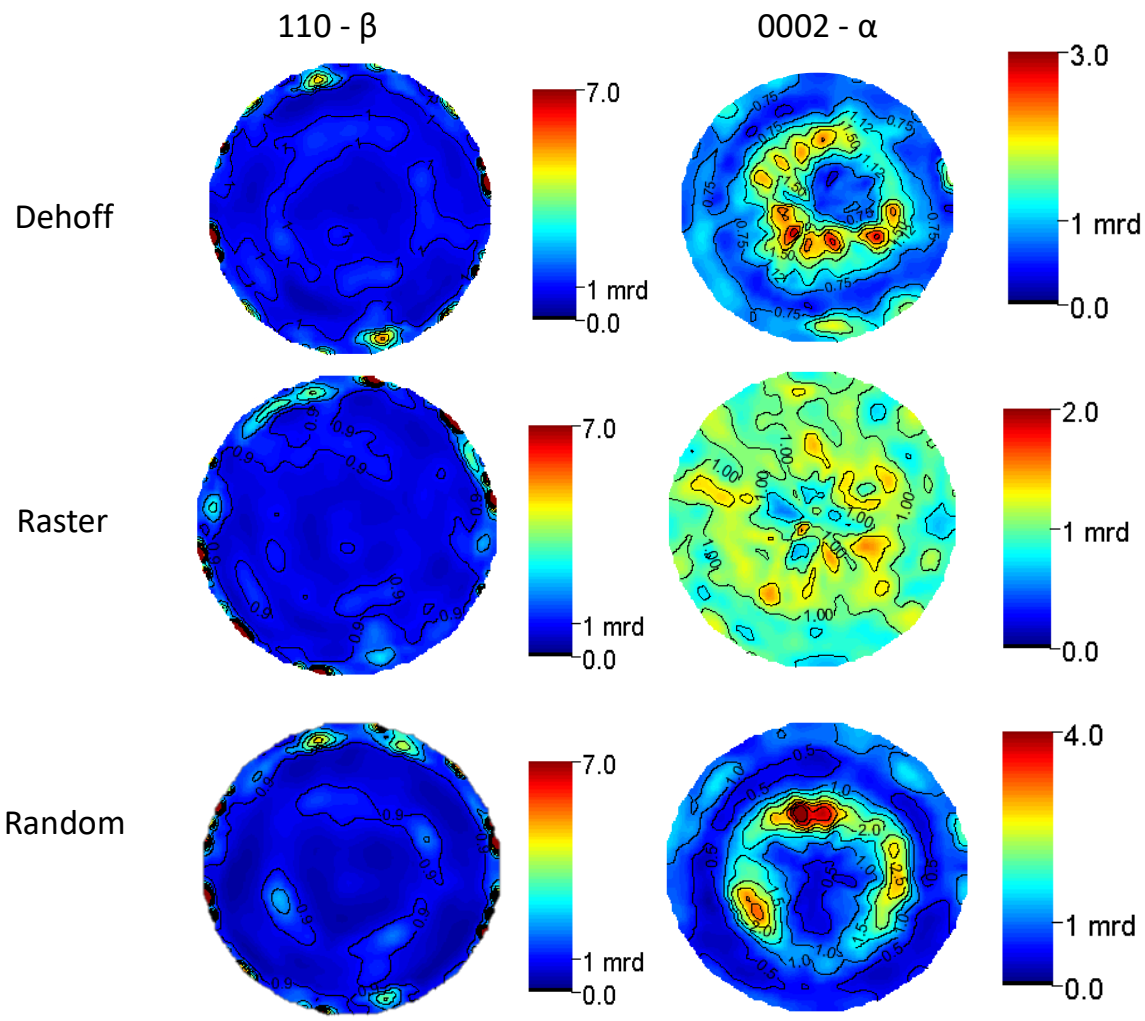

Figure 36.4: Pole figures the α and β titanium phases in Ti-6Al-4V samples processed with three different scan strategies. A stronger (0002) α phase texture is observed in both the DeHoff (top) and Random (bottom) scan strategies compared to the Linear Raster scan strategy. Note the mrd scale is different for each plot.

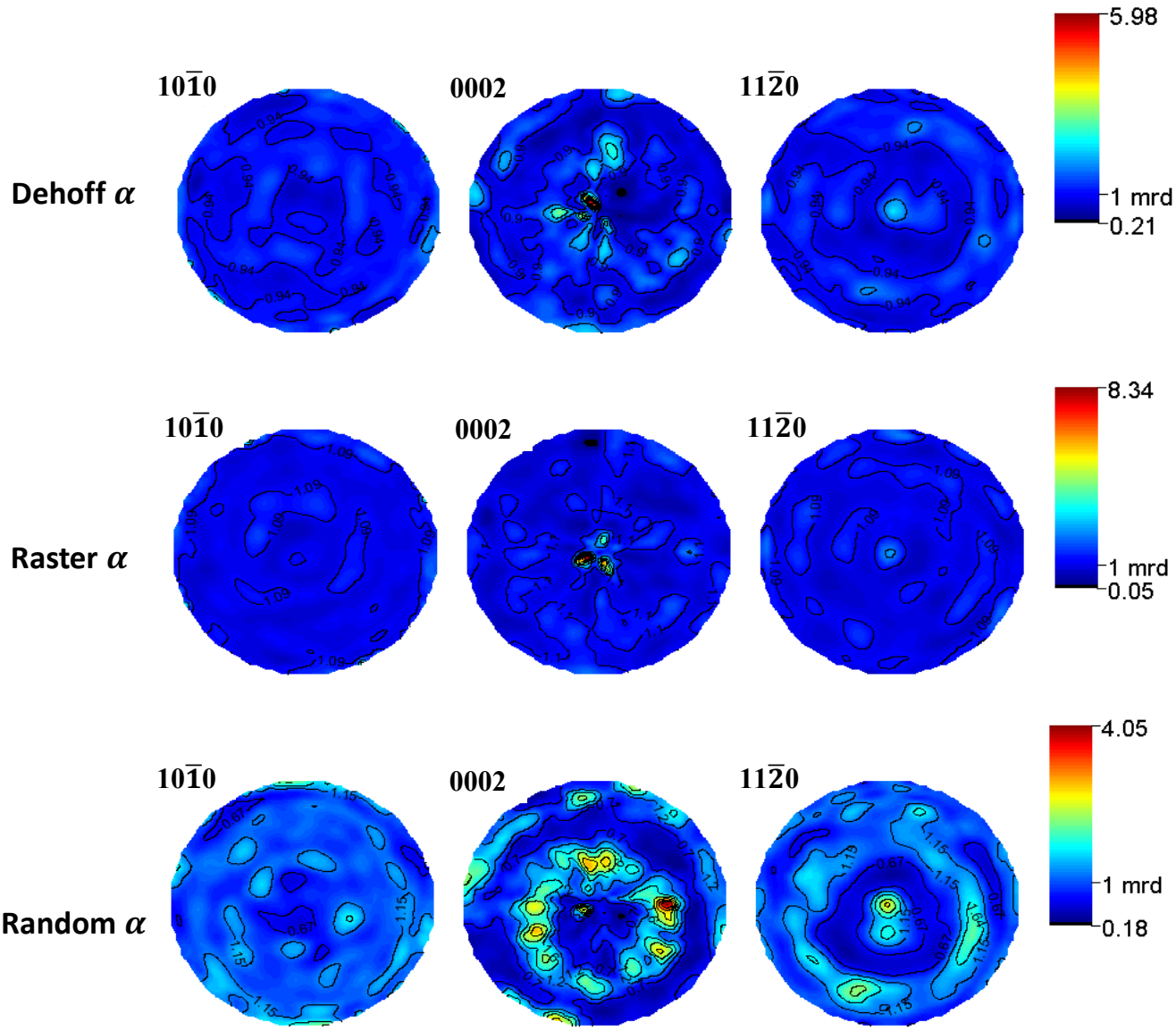

Figure 36.5: Local texture pole figures of α titanium taken 1 mm from the initial build surface for each scan strategy of interest. Note the higher intensities of (0002) texture in the Linear Raster and Dehoff scan strategies. Note the mrd scale is different for each plot.

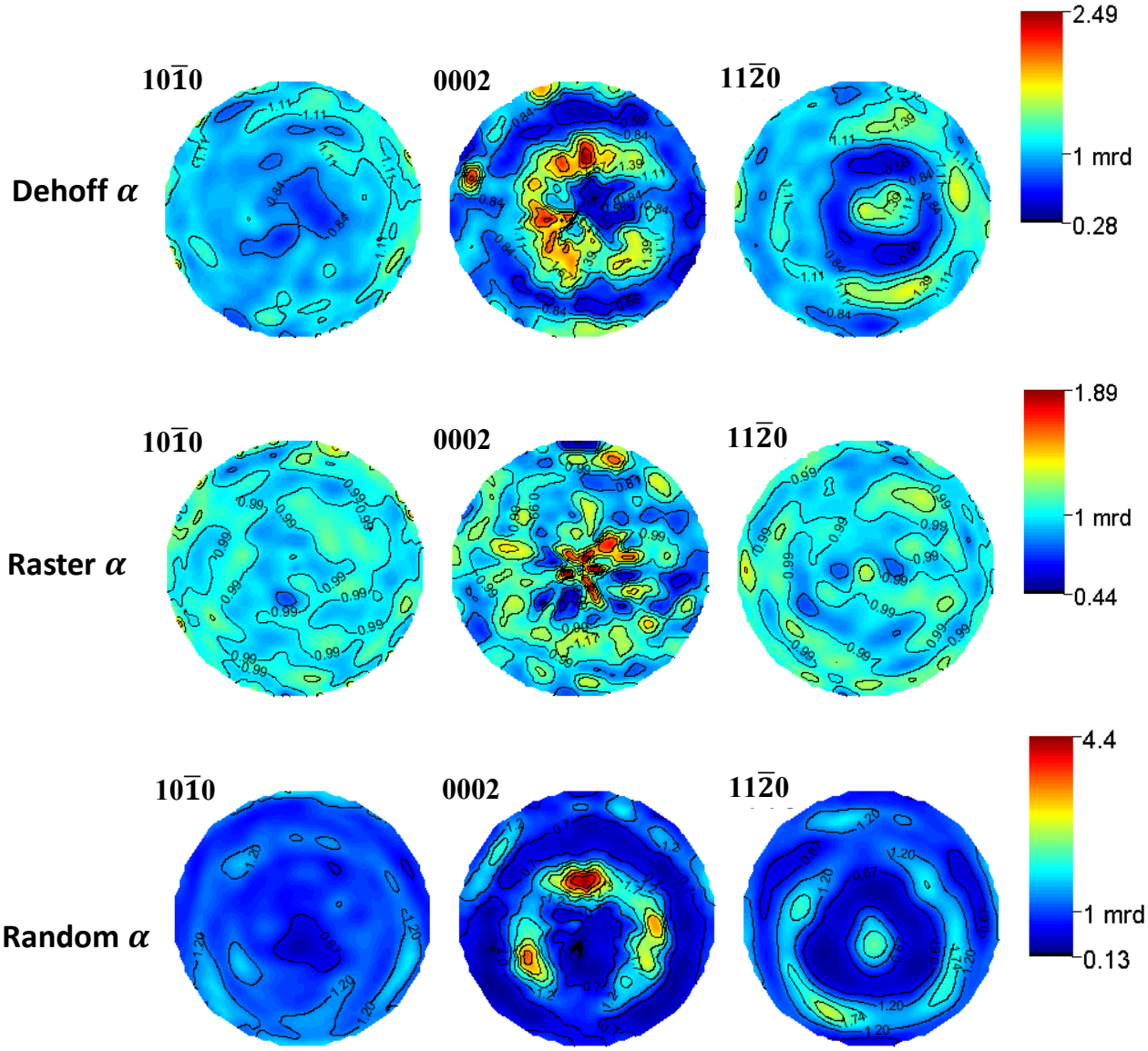

Figure 36.6: Local texture pole figures of α titanium taken 13 mm from the initial build surface for each scan strategy of interest. Note the sharply reduced texture intensities of the raster and Dehoff strategies along with the slight increase in clustering in the Random strategy compared to 1 mm above the build surface (**Figure 36.5**). Note the mrd scale is different for each plot.

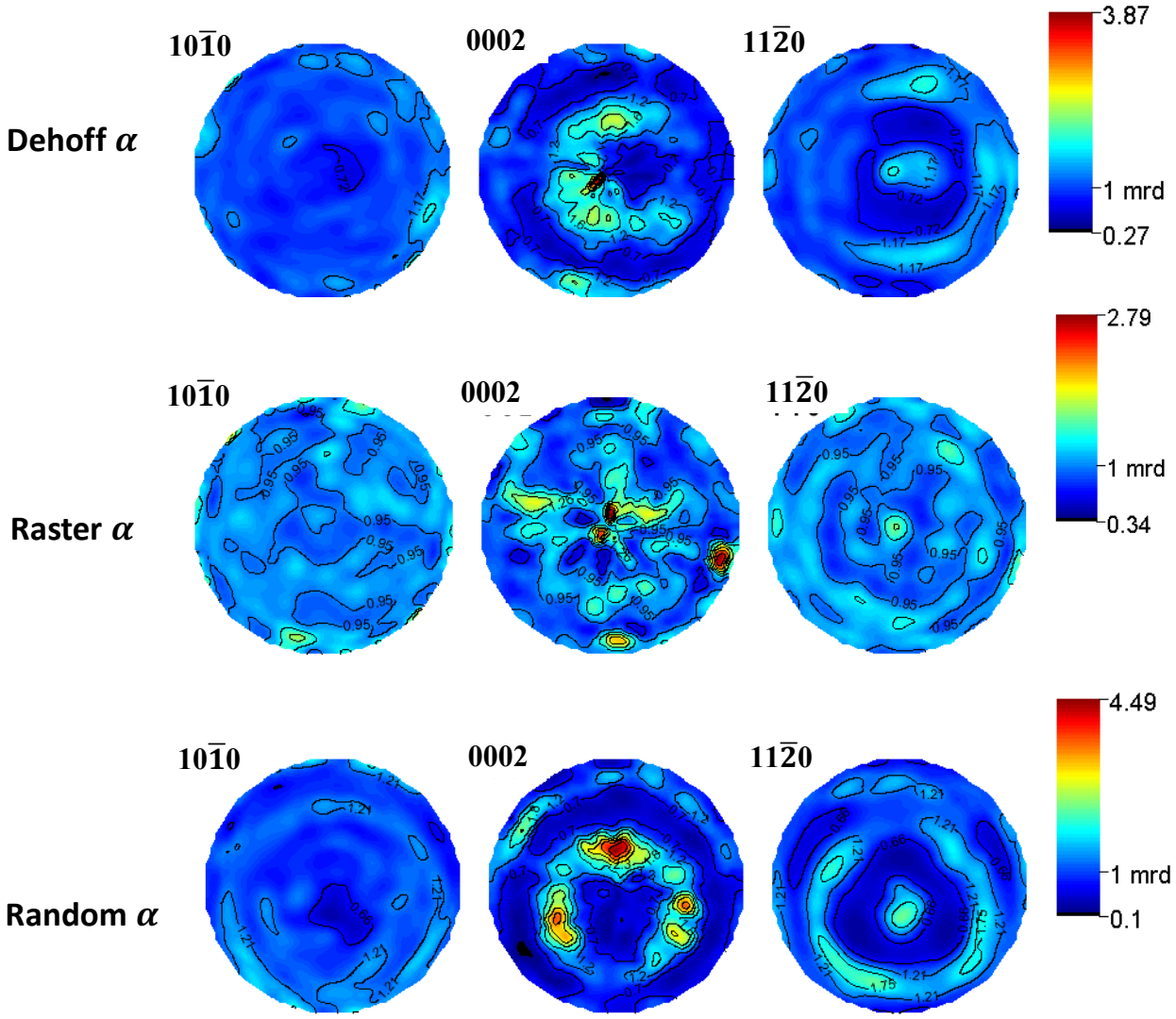

Figure 36.7: Local texture pole figures of α titanium taken 24 mm from the initial build surface for each scan strategy of interest. Note the consistency of the Random scan strategy and the differences in texture profiles of the Linear Raster and Dehoff strategies compared to **Figure 36.6**. Note the mrd scale is different for each plot.